Discrimination Between Diastereoisomeric Dipeptides by IR–UV Double Resonance Spectroscopy and Ab Initio Calculations

ALI G. ABO-RIZIQ, JOHN E. BUSHNELL, BRIDGIT CREWS, MICHAEL P. CALLAHAN, LOUIS GRACE, MATTANJAH S. DE VRIES

Department of Chemistry and Biochemistry, University of California, Santa Barbara, California 93106

Received 10 May 2005; accepted 10 May 2005
Published online 14 July 2005 in Wiley InterScience (www.interscience.wiley.com).
DOI 10.1002/qua.20719

ABSTRACT: We studied diastereoisomeric dipeptides, containing two chiral centers, by comparing ab initio calculations with laser desorption jet-cooling experiments. We studied the hetero-dipeptides LL–VF (L-Val-L-Phe) and DL–VF and the homo-dipeptides LL–FF (L-Phe-L-Phe) and LD–FF. Changing one of the chiral centers in each molecule leads to changes in the spectra that can be used to distinguish between diastereoisomeric pairs. We observed three different conformers for LL–VF, four for DL–VF, two for LL–FF, and one for LD–FF. By comparing the results from IR–UV double resonant spectroscopy with ab initio calculations, we can draw conclusions about the conformational structures. At the same time, the experimental data serve as a test for the computational results. We discuss the possibilities and limitations of the interplay between theory and experiment. Int J Quantum Chem 105: 437–445, 2005

Key words: R2PI; UV–UV hole burning; IR–UV double resonance spectroscopy; ab initio calculations; diastereoisomers

Correspondence to: M. S. de Vries; e-mail: devries@chem.ucsb.edu.

Contract grant sponsor: American Chemical Society Petroleum Research Fund.

Introduction

Computational chemistry describes molecules of increasing size with increasing levels of accuracy, including DNA bases and small peptides. With this success comes the need for gas-phase experimental data for calibration of force fields and testing of new algorithms and methods. The experimental study of individual molecules is the prime domain of gas-phase techniques, which can provide the best data for comparison with theory. Until recently, biomolecular building blocks and related molecules could not be studied in the gas phase for practical reasons. Experimentally, these compounds have very low vapor pressures, and they decompose when heated. At the same time, computationally these systems are also challenging, since often correlation or dispersion energy would have to be included to describe them properly. This means that semi-empirical quantum chemical methods, and even ab initio Hartree–Fock (HF) and density functional theory (DFT) methods, are not always sufficient. In both areas, significant progress has now been made, making direct comparison possible between gas-phase experimental data and computations. As one example of the possibilities and limitations of this approach, we studied diastereoisomeric dipeptides, containing two chiral centers, and compared ab initio calculations with laser desorption jet-cooling experiments.

Chirality and chiral molecules are essential concepts in chemistry and biology. In biology, most living organisms are composed of chiral molecules such as amino acids, sugars, nucleic acids, and proteins [1]. One of the major mysteries in nature is that all amino acids in proteins are "left-handed" enantiomers, while all sugars in DNA and RNA are "right-handed" enantiomers [2, 3]. Diastereomers arise in compounds that have more than one chiral center, but they are not necessarily mirror images of each other. Diastereomers have different physical properties, which can lead to different conformational preferences and functional activity. Chirality plays an important role for living organisms. Thus it has become a major concern in drug design, including the need to distinguish and separate enantiomers and diastereomers. Gas-phase laser spectroscopy offers a great opportunity to study conformations of these molecules free of a solvent environment.

Simons and colleagues [4, 5] studied the neurotransmitter ephedrine and its diastereoisomer pseudoephedrine. Both molecules contain two chiral centers connected by one covalent bond. The resonant two-photon ionization (R2PI) spectra of both molecules showed significant differences, and by obtaining the ultraviolet (UV)–UV hole burning spectra, they found two different conformers for ephedrine and four conformers for the other diastereoisomer. The major difference in these two molecules arises from intramolecular hydrogen bonding, which leads to different conformational preferences for each diastereoisomer.

Recently several groups have been studying chiral complexes in the gas phase by means of laser-induced fluorescence (LIF) spectroscopy, (R2PI) spectroscopy, and UV–UV double resonance spectroscopy [6–11]. They form stable, weakly bound diastereoisomeric clusters of an aromatic chiral molecule with different chiral solvents in a supersonic beam expansion. These studies show distinguishable differences in the R2PI spectra of homochiral (RR or SS) and heterochiral (RS or SR) complexes. By measuring the dissociation energies of the different complexes, the authors find that the homochiral clusters are more stable than the heterochiral clusters.

In previous gas-phase studies on chiral molecules, the molecules were introduced into the gas phase by heating. Nonvolatile molecules such as peptides fragment easily upon heating. Laser desorption with subsequent jet cooling, which quickly vaporizes and cools the molecules before they can fragment, provides a powerful technique to study these fragile molecules. Here we report the study of two pairs of diastereoisomeric dipeptides LL–FF and LD–FF, and LL–VF and DL–VF. The structures of these molecules are shown in Figure 1. We are particularly interested in the short-range molecular interactions, such as intramolecular hydrogen bonding and dispersion forces that may lead to differences in the structure and vibronic spectra of these molecules. To study these interactions, one needs to isolate and determine the structures of each diastereoisomer.

Experimental Method

The experimental setup has been described elsewhere [12]. All chemicals were obtained from Research Plus Co. and used without further purification. In brief, we prepare the samples by crushing the neat dipeptides onto the surface of a graphite substrate. To bring the molecules into the gas

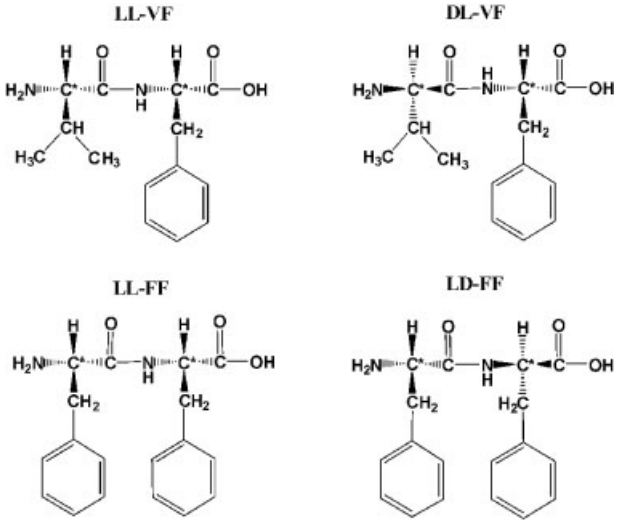

FIGURE 1. Structures of the two pairs of diastereoisomers, LL–VF, DL–VF, and LL–FF, LD–FF. The stars represent the chiral centers of each molecule.

phase, we desorb them using a Nd:YAG laser operating at its fundamental wavelength (1,064 nm). We attenuate the laser to 1 mJ/cm^2 and then focus on a spot of ~0.5 mm diameter within 2 mm in front of the nozzle. To maximize the stability of desorption from pulse to pulse, the sample sits on a translational stage and moves at such a rate as to ensure that fresh sample is desorbed in each shot. The nozzle consists of a pulsed valve with an orifice diameter of 1 mm, and is operated at a stagnation pressure of ~5 atm of argon drive gas.

To obtain an R2PI spectrum, we use a tunable dye laser in the UV region from 264 to 268 nm. By monitoring specific mass peaks while varying the two-photon ionization wavelength, we obtain the mass selected excitation spectra (R2PI spectra). We record UV–UV double resonance spectra by applying a delay of ~200 ns between two dye laser pulses. As a result of this delay in time, we obtain two peaks in the time-of-flight spectrum, which can be monitored individually. The laser that fires first serves as an intense "burn" laser and is scanned over the R2PI spectrum region, while the delayed laser serves as the "probe" laser, fixed on one resonance. When both lasers are tuned to a resonance of the same conformer, the result is a decrease in the signal of the probe laser. With this technique we can determine the origins and the number of conformers for each molecule. To obtain the infrared (IR) spectrum for each conformer, we use IR–UV double resonance spectroscopy. The IR laser functions as the "burn" laser pulse, preceding the UV "probe" laser pulse by ~100 ns. The UV laser is tuned to a resonance of a specific conformer, and the IR laser is scanned. When the IR laser is resonant with a vibrational transition that belongs to the same conformer, it causes a depletion of the ground state, which leads to a decrease in the intensity of the ion signal. The IR is produced by an OPO system (LaserVision) pumped by a Nd:YAG laser (Quanta-Ray) operated at its fundamental wavelength of 1,064 nm. For this work, we operated within the range of 3200–3700 cm^{-1}, which encompasses NH, NH_2, and OH modes. The output of the OPO system is 8 mJ/pulse, and the bandwidth is 3 cm^{-1}.

Theoretical Method

We performed calculations on neutral dipeptides using a two-step approach. We first calculated candidate structures using a simple molecular mechanics force field followed by geometry optimization using DFT. We used the AMBER force field to perform simulated annealing on each dipeptide as implemented in the Amber 7 program suite [13]. We then selected ~100 low-energy candidate structures from Amber, which were then used as starting structures for subsequent optimization with the B3LYP [14–17] hybrid density functional with the Gaussian 03 program [18].

We build the preliminary structures of the peptides using the xleap program of Amber 7. We then adjust the conformations for the desired L or D form, and modify the default zwitterion structure to the neutral (gas-phase) structure. These structures are minimized in Gaussian 03 by means of the B3LYP functional and the 6-31G* basis set in order to generate the charges needed in Amber. We use the *antechamber* program of Amber 7 to generate charges from the Gaussian 03 output. The charges are calculated only for a single conformation, but they are only used to calculate candidate structures with simulated annealing. We perform simulated annealing by using a simple protocol of running at high temperature (800 K) for 30 ps followed by 10 ps of stepwise cooling, and a final energy minimization. We typically repeat this cycle 500 times, sort the results by energy, and classify them according to structure.

We chose ~100 lower-energy candidate structures of each molecule for subsequent optimization in Gaussian 03. We minimized these by means of

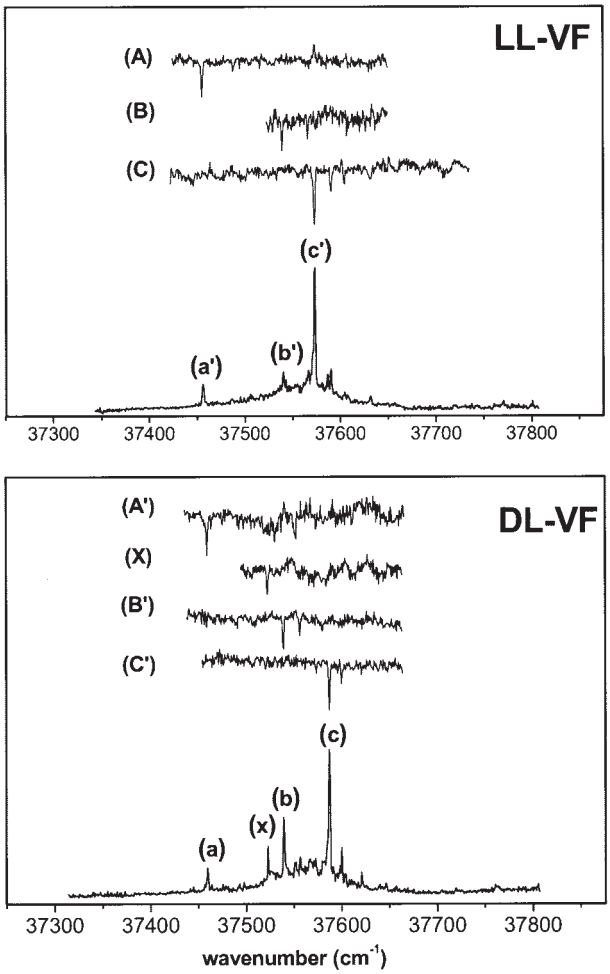

FIGURE 2. R2PI spectra and UV–UV double resonant spectra of LL–VF (top) and DL–VF (bottom).

the B3LYP density functional and the 6-31G* basis set. From these, we chose 30 candidate structures of each molecule for optimization using a higher basis set (6-311G**). As a final step, we calculated the normal mode frequencies of all these structures for comparison with the experimental data. The frequencies were scaled by a uniform factor of 0.956, based on the experimental versus calculated frequency ratios for single unshifted free OH peaks [19–21].

Results and Discussion

LL–VF AND DL–VF

Figure 2 shows the R2PI spectra of LL–VF and DL–VF (bottom trace, top and bottom, respectively). Significant differences can be seen in the R2PI spectra. Peak (a′), the red-most peak in LL–VF, is 3 cm^{-1} to the red relative to peak (a) in DL–VF. Peaks (b) and (b′) are in the same position, but (b) is more intense than (b′). The most intense peak in LL–VF, (c′), is 14 cm^{-1} to the red of (c). The peak marked (x) in DL–VF does not have an equivalent in the spectrum of the other diastereoisomer.

Figure 2 also shows the UV–UV double resonance spectra. The top traces represent the UV–UV spectra recorded with the probe laser tuned to an intense transition of each conformer. We observed three different conformers for LL–VF and four conformations for DL–VF. We found that peak (x), which is not present for LL–VF, is the origin of a separate conformer. All conformers exhibit different low-energy (torsional) vibrations from those in the corresponding conformer of the other diastereoisomer. For example, the first vibration of conformer (C) in LL–VF lies 16 cm^{-1} to the blue of the origin, while in the corresponding conformer in DL–VF (C′), it lies 11 cm^{-1} from the origin.

Figure 3(a) and 3(b) show the most stable structures of LL–VF and DL–VF, respectively, calculated by means of the B3LYP functional with 6-311G** basis set. The global minimum for both molecules shows a hydrogen bond between the hydroxyl of the C-terminus and the carbonyl of the peptide bond. The relative energy of each structure is given above each structure in kcal/mol.

To determine the possible structures of the different conformers of each molecule, we performed IR–UV double resonance spectroscopy and compared the experimental frequencies with those that we calculated for each structure shown in Figure 3(a) and 3(b) for LL–VF and DL–VF. Figure 4 shows the IR–UV double resonance spectra of LL–VF. The bottom bar spectra represent the calculated frequencies for the structures that are presented in Figure 3(a). The top traces are the experimental spectra obtained by IR–UV double resonance spectroscopy. It is important to note that the differences in the calculated spectra are very small. Thus it is very difficult to determine the exact structure for each conformer at the level of calculation that we are using.

We scanned the IR laser from 3,650 to 3,250 cm^{-1}, searching for the carboxylic hydroxyl, the NH, and the NH_2 symmetric and antisymmetric stretch frequencies. For conformers (B) and (C) of this molecule, we observed the hydroxyl stretch at 3,590 cm^{-1}, which is typical for the free hydroxyl of carboxylic acid groups in peptides. The NH stretch

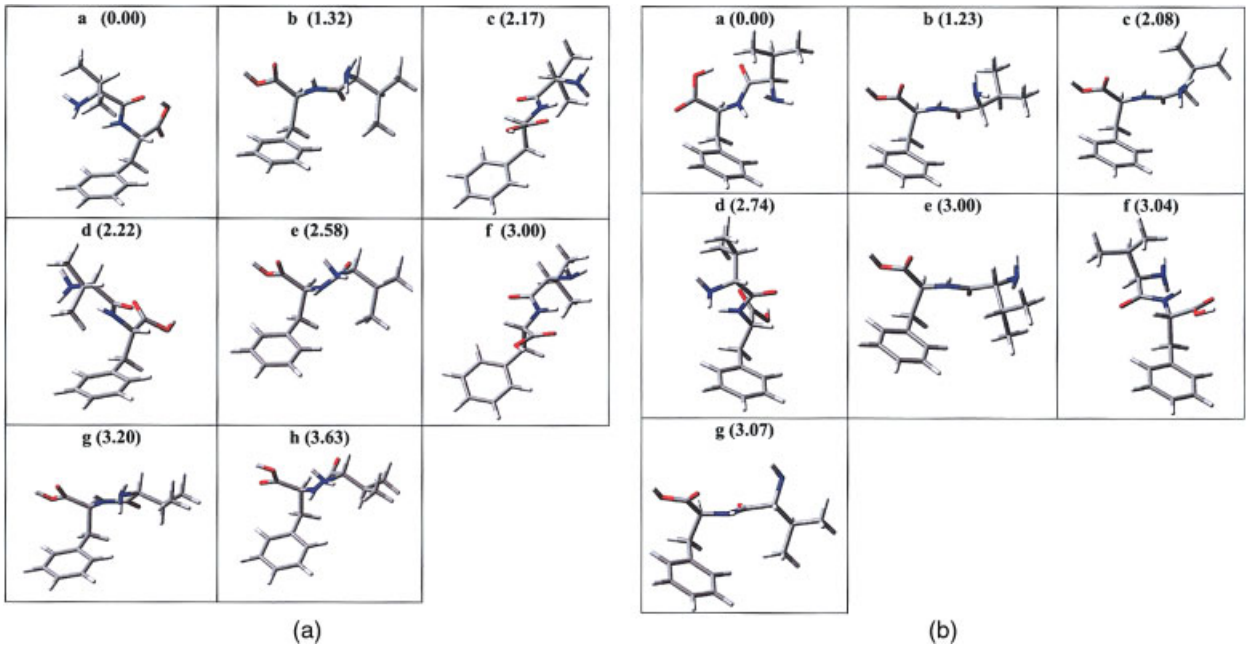

FIGURE 3. (a) Lowest-energy conformations as calculated by DFT/6311G** for LL–VF. The relative energy in kcal/mol is listed above each structure. (b) Lowest-energy conformations as calculated by DFT/6311G** for DL–VF. The relative energy in kcal/mol is listed above each structure. [Color figure can be viewed in the online issue, which is available at www.interscience.wiley.com.].

mode in conformers (B) and (C) appears at 3,407 cm^{-1} and 3,409 cm^{-1}, respectively. For conformer (A), the hydroxyl frequency appears ~13 cm^{-1} to the red compared with that in conformers (B) and (C). Structure a, in Figure 3(a), is the global minimum structure calculated for this molecule. For this conformer, the strong hydrogen bond between the hydroxyl and the carbonyl of the peptide bond would result in a red shift of the hydroxyl frequency by >400 cm^{-1}. Because we do not observe this experimentally, we can exclude this structure as a candidate. For conformer (A), there are three possible structures: c, f, and h. The frequencies are comparable to the extent that we cannot distinguish among these structures based on the calculations. In each of these structures, the hydroxyl is positioned above the benzene ring of the phenylalanine residue. This position can lead to a weak interaction of the hydroxyl with the π system of the ring. This weak interaction can explain the small red shift of the hydroxyl frequency for conformer (A) compared to that in conformers (B) and (C). Structures b, d, e, and g are candidate structures for conformers (B) and (C), and it is not possible to choose two unique assignments from among the four candidate structures.

Figure 5 shows the IR–UV spectra of the four different conformers that we found for DL–VF, and compares them with the calculated frequencies of the structures from Figure 3(b) that were optimized. From the IR spectra, we once again determine that the hydroxyl at the carboxylic C-terminus is free, as in the other diastereoisomer, LL–VF. The frequency of the hydroxyl in conformer (A′) of DL–VF is 15 cm^{-1} to the red relative to the hydroxyl in the other conformers of this molecule. This shift is very similar to that for conformer (A) of LL–VF. From our comparison of the experimental IR frequencies and the calculated frequencies for the different structures of this molecule, we tentatively propose structure f in Figure 3(b) as the best match, considering the frequencies and intensities. We see that the intensity of the hydroxyl mode is noticeably smaller than the intensity of the NH stretch mode of the peptide bond, which we observe at 3,409 cm^{-1}. In addition, we observe a very weak transition at 3,433 cm^{-1}, which we believe belongs to the NH_2 antisymmetric stretch based on comparison with the calculated frequencies of structure f.

We observe the stretch of the hydroxyl in conformers (X), (B′), and (C′) at 3,592 cm^{-1}, which is typical for the free hydroxyl in peptides. The NH

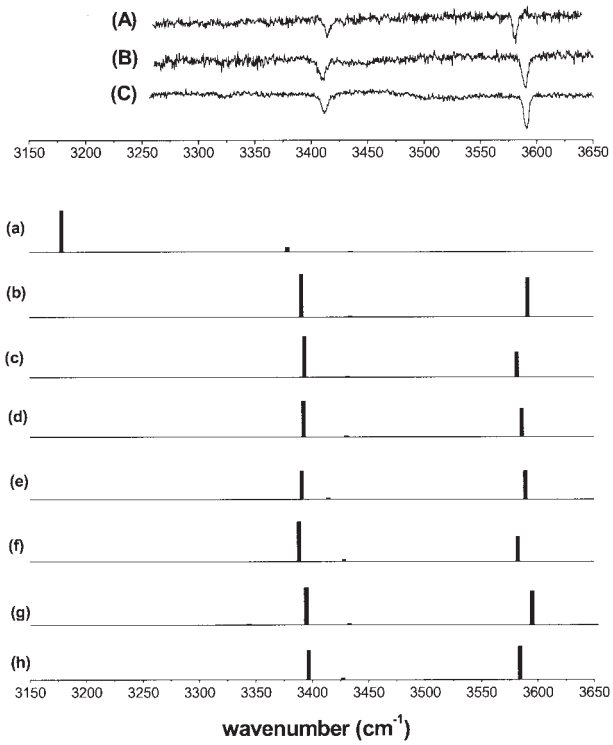

FIGURE 4. Experimental IR–UV double resonance spectra of the three different conformers of LL–VF, compared with calculated frequencies for the eight structures from Fig. 3(a). The frequencies were scaled by factor of 0.956.

stretch modes of the amide groups appear at 3,403, 3,405, and 3,409 cm^{-1}, respectively, which are typical frequencies for a free amide group. The NH_2 antisymmetric stretch for conformer (X) is measured at 3,430 cm^{-1}, and for conformer (C′) it is measured at 3,438 cm^{-1}. For conformer (B′), we did not observe this band. This may be due to its low intensity, since frequency calculations show that the intensity of NH_2 symmetric and antisymmetric modes are very close to zero and in many cases are zero. By comparing the IR spectra of these three conformers with the calculated frequencies, we can exclude structure a, which is the global minimum of DL–VF predicted by DFT. The strong hydrogen bonding between the hydroxyl and the carbonyl of the amide in this conformer would cause a large red shift of the hydroxyl frequency, which is not observed experimentally. The frequencies of conformer (X) fit best with the frequencies of structure c. Conformer (B′) fits best with structure g, and conformer (C′) fits best with structure e. These tentative assignments are based both on the positions of the different bands and on their relative intensities.

LL–FF AND LD–FF

Figure 6 shows the R2PI spectra and UV–UV double resonance spectra of LL–FF (top) and LD–FF (bottom). For LL–FF, we observed two conformers, of which conformer (A) exhibits all sharp peaks in the R2PI spectrum. The spectrum for conformer (B) was difficult to resolve because its origin is so weak. This suggests that the molecule undergoes a large geometry change during excitation. The most intense peak for this conformer, which is marked by a star, is mixed with a peak that belongs to conformer (A). To resolve this peak, we had to set the burn laser at different points on the two mixed peaks until we obtained the double resonance spectrum that most clearly contained peaks that belong only to conformer (B). For LD–FF, we found one conformer and, as we observe for conformer (B) of LL–FF, the intensity of the origin is very weak

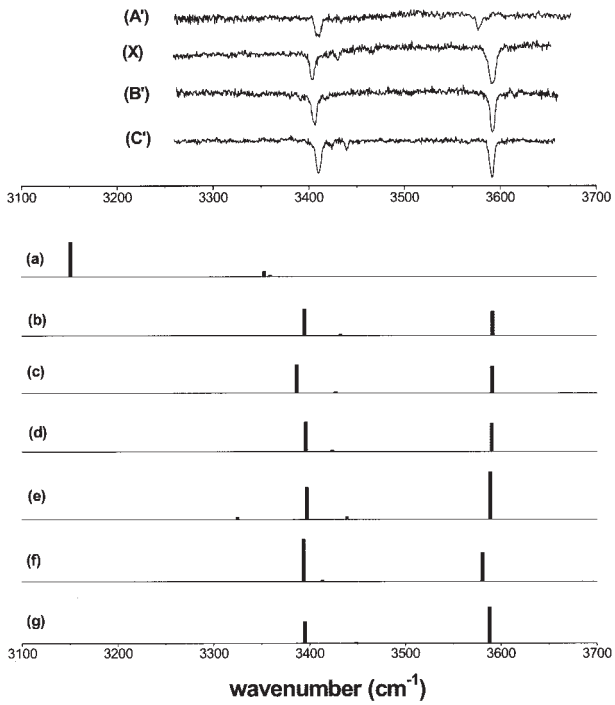

FIGURE 5. Experimental IR–UV double resonance spectra of the four different conformers of DL–VF, compared with calculated frequencies for the seven structures from Fig. 3(b). The frequencies were scaled by factor of 0.956.

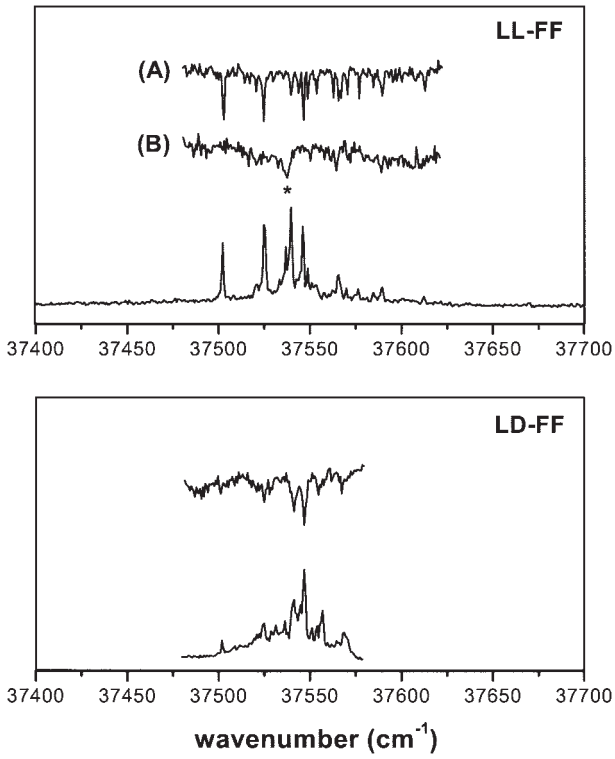

FIGURE 6. R2PI and UV–UV double resonance spectra for LL–FF (top). The star represents the peak in which the probe laser was tuned on conformer (B) while we scanned the burn laser. This peak is not the origin for this conformer. R2PI and UV–UV double resonance spectra for LD–FF (bottom).

compared with the intensity of the low-frequency vibrational bands.

Figure 7(a) and 7(b) show the calculated structures for LL–FF and LD–FF, respectively, calculated by means of the B3LYP functional with the 6-311G** basis set. The global minimum for both molecules shows a hydrogen bond between the hydroxyl of the C-terminus and the carbonyl of the peptide bond. The relative energy of each structure is given above each structure in kcal/mol.

Figure 8 shows the IR–UV double resonance spectra and calculated frequencies for LL–FF. As before, the experimental spectra are at the top, and the calculated spectra are at the bottom. The IR spectra of both conformers show strong transitions at 3,591 cm^{-1}, which is typical for the free hydroxyl stretch. We can therefore exclude structure a, in Figure 7(a), as a possible conformer. Conformer (A) shows another peak at 3,413 cm^{-1}, which is typical for the free NH of the amide. The most probable candidate structure for this conformer is structure c, which is an unfolded structure in which the two benzyl groups of the phenylalanine residues are spread away from each other. In conformer (B), we measured the NH stretch of the amide group at 3,405 cm^{-1}, and in addition to this transition we observe a small peak at 3,411 cm^{-1}, which originates from the NH_2 antisymmetric stretch. The spectrum calculated for structure b has the best fit to the spectrum for this conformer. This structure is the second most stable and, based on the calculations, it is higher in energy by 0.25 kcal/mol relative to the predicted global minimum structure. In this structure, the benzene rings of the two phenylalanine residues are perpendicular to each other. As a result, the hydrogens of the phenylalanine ring on

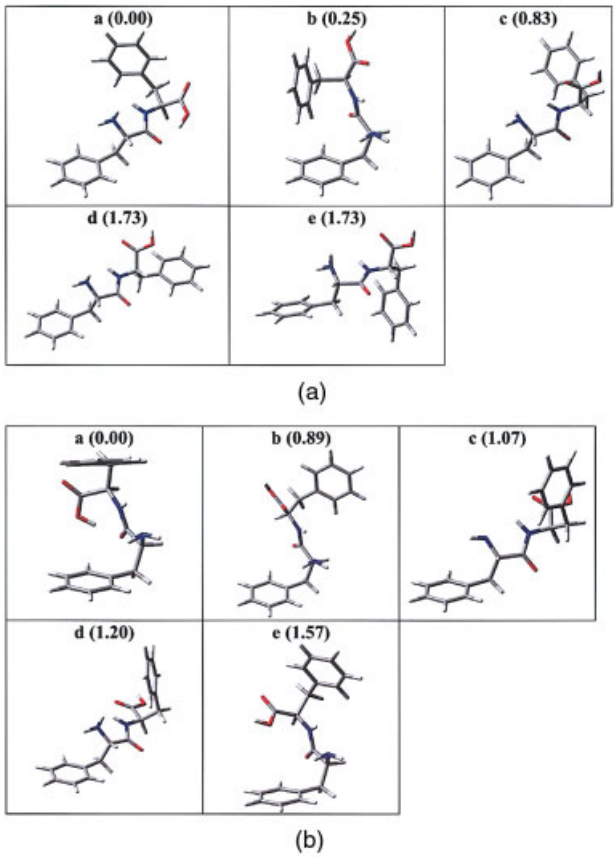

FIGURE 7. (a) Lowest-energy conformations as calculated by DFT/6311G** for LL–FF. The relative energy in kcal/mol is listed above each structure. (b) Lowest-energy conformations as calculated by DFT/6311G** for LD–FF. The relative energy in kcal/mol is listed above each structure. [Color figure can be viewed in the online issue, which is available at www.interscience.wiley.com.].

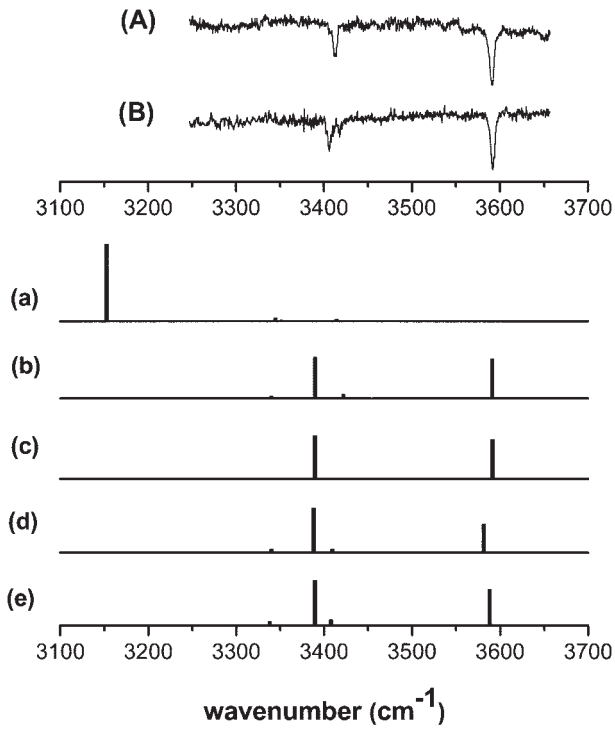

FIGURE 8. Experimental IR–UV double resonance spectra of the two different conformers of LL–FF, compared with calculated frequencies for the five structures from Fig. 7(a). The frequencies were scaled by factor of 0.956.

the C-terminus interact with the π electrons of the phenylalanine on the N-terminus.

Figure 9 shows the IR spectra and the calculated frequencies for the diastereoisomer LD–FF. This molecule has just one conformer, which is similar to conformer (B) of LL–FF, both in its R2PI spectrum and in its IR–UV spectrum. The hydroxyl stretch is at 3,591 cm^{-1}. As was the case for both conformers of LL–FF, we can exclude the global minimum structure as the experimentally observed structure. The NH stretch mode of the amide is at 3,402 cm^{-1}, 3 cm^{-1} to the red relative to that of conformer (B) in LL–FF, and the NH_2 antisymmetric stretch is at 3,411 cm^{-1}. Comparison of the frequencies of this molecule with the calculated frequencies shows that structure c in Figure 7(b) fits best.

Summary

The study of small peptides such as the dipeptides discussed in the present study provides an example of the interplay between theory and experiment for molecules of moderate size. The parameters for comparison in this example are the frequencies and intensities of conformer-selective IR spectra. The results point to both strengths and limitations. The agreement between theory and experiment is very encouraging; however, for conformations with very similar vibrational frequencies, the computational accuracy employed here is not sufficient to make a unique structural assignment in all cases. It is also clear that because full structural optimization is computationally expensive, a strategy is needed to search for lowest-energy structures. Another problem is the role of dispersive forces, which cause problems for DFT-based treatments.

Nevertheless, because both experiment and theory are advancing simultaneously in their ability to tackle larger and larger systems, great progress is being made in the description of molecules of every increasing size. This has led to a great synergy between the two areas. The question then suggests itself as to what the size limit will be for these approaches. Experimentally, a potential problem

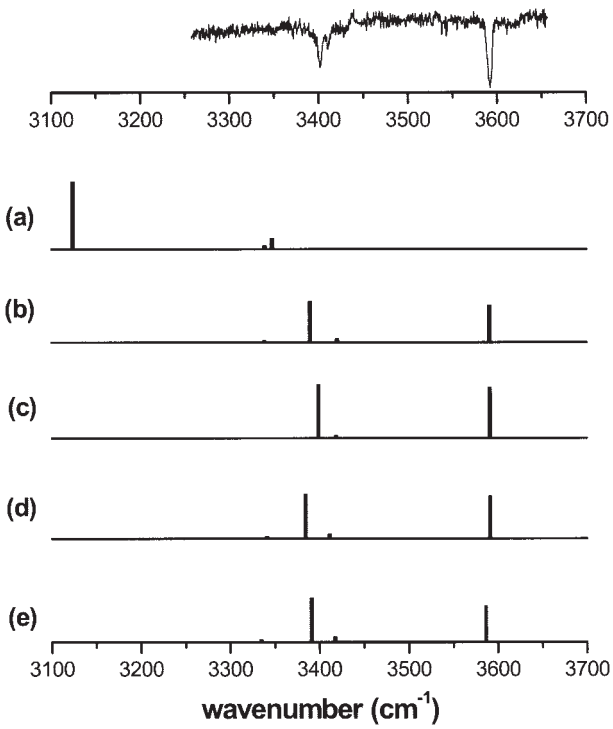

FIGURE 9. Experimental IR–UV double resonance spectrum of LD–FF, compared with calculated frequencies for the five structures from Fig. 7(b). The frequencies were scaled by factor of 0.956.

may be conformational broadening. Even with broad UV absorption, however, it may still be possible to obtain sharp IR spectra in many cases. Furthermore, our experimental results indicate that even for peptides with as few as four residues, there may often be a single preferred conformation in the gas phase.

Finally, we note that the spectroscopic distinction between diastereoisomeric dipeptides, as demonstrated here, offers opportunities for analytical applications.

ACKNOWLEDGMENT

Acknowledgment is made to the Donors of the American Chemical Society Petroleum Research Fund for support of this research.

References

1. Ulbricht, T. L. V. Nature 1975, 258, 383.
2. Yuasa, S. J Biol Phys 1994, 20, 229.
3. Saghatelian, A.; Yokobayashi, Y.; Soltani, K.; Ghadiri, M. R. Nature 2001, 409, 797.
4. Butz, P.; Kroemer, R. T.; Macleod, N. A.; Simons, J. P. J Phys Chem A 2001, 105, 544.
5. Butz, P.; Kroemer, R. T.; Macleod, N. A.; Robertson, E. G.; Simons, J. P. J Phys Chem A 2001, 105, 1050.
6. Alrabaa, A. R.; Breheret, E.; Lahmani, F.; Zehnacker, A. Chem Phys Lett 1995, 237, 480.
7. Alrabaa, A.; LeBarbu, K.; Lahmani, F.; ZehnackerRentien, A. J Phys Chem A 1997, 101, 3273.
8. Piccirillo, S.; Bosman, C.; Toja, D.; GiardiniGuidoni, A.; Pierini, M.; Troiani, A.; Speranza, M. Angew Chem Int Ed Engl 1997, 36, 1729.
9. Le Barbu, K.; Brenner, V.; Millie, P.; Lahmani, F.; Zehnacker-Rentien, A. J Phys Chem A 1998, 102, 128.
10. Guidoni, A. G.; Piccirillo, S.; Scuderi, D.; Satta, M.; Di Palma, T. M.; Speranza, M. Phys Chem Chem Phys 2000, 2, 4139.
11. Mons, M.; Piuzzi, F.; Dimicoli, I.; Zehnacker, A.; Lahmani, F. Phys Chem Chem Phys 2000, 2, 5065.
12. Meijer, G.; Devries, M. S.; Hunziker, H. E.; Wendt, H. R. Appl Phys B Photophys Laser Chem 1990, 51, 395.
13. Case, D. A.; Pearlman, D. A. P.; Caldwell, J. W.; Cheatham, T. E., III; Wang, J.; Ross, W. S.; Simmerling, C. L.; Darden, T. A.; Merz, K. M.; Stanton, R. V.; Cheng, A. L.; Vincent, J. J.; Crowley, M.; Tsui, V.; Gohlke, H.; Radmer, R. J.; Duan, Y.; Pitera, J.; Massova, I.; Seibel, G. L.; Singh, U. C.; Weiner, P. K.; Kollman, P. A. Amber 7; University of California: San Francisco, 2002.
14. Stephens, P. J.; Devlin, F. J.; Chabalowski, C. F.; Frisch, M. J. J Phys Chem 1994, 98, 11623.
15. Becke, A. D. J Chem Phys 1993, 98, 5648.
16. Becke, A. D. Phys Rev A 1988, 38, 3098.
17. Lee, C. T.; Yang, W. T.; Parr, R. G. Phys Rev B 1988, 37, 785.
18. Frisch, M. J.; Trucks, G. W.; Schlegel, H. B.; Scuseria, G. E.; Robb, M. A.; Cheeseman, J. R.; Montgomery, J. A., Jr.; Vreven, T.; Kudin, K. N.; Burant, J. C.; Millam, J. M.; Iyengar, S. S.; Tomasi, J.; Barone, V.; Mennucci, B.; Cossi, M.; Scalmani, G.; Rega, N.; Petersson, G. A.; Nakatsuji, H.; Hada, M.; Ehara, M.; Toyota, K.; Fukuda, R.; Hasegawa, J.; Ishida, M.; Nakajima, T.; Honda, Y.; Kitao, O.; Nakai, H.; Klene, M.; Li, X.; Knox, J. E.; Hratchian, H. P.; Cross, J. B.; Adamo, C.; Jaramillo, J.; Gomperts, R.; Stratmann, R. E.; Yazyev, O.; Austin, A. J.; Cammi, R.; Pomelli, C.; Ochterski, J. W.; Ayala, P. Y.; Morokuma, K.; Voth, G. A.; Salvador, P.; Dannenberg, J. J.; Zakrzewski, V. G.; Dapprich, S.; Daniels, A. D.; Strain, M. C.; Farkas, O.; Malicj, D. K.; Rabuck, A. D.; Raghavachari, K.; Foresman, J. B.; Ortiz, J. V.; Cui, Q.; Baboul, A. G.; Clifford, S.; Cioslowski, J.; Stefanov, B. B.; Liu, G.; Liashenko, A.; Piskorz, P.; Komaromi, I.; Martin, R. L.; Fox, D. J.; Keith, T.; Al-Laham, M. A.; Peng, C. Y.; Nanayakkara, A.; Challacombe, M.; Gill, P. M. W.; Johnson, B.; Chen, W.; Wong, M. W.; Gonzalez, C.; Pople, J. A. Gaussian 03, revision B.04; Gaussian: Pittsburgh, PA, 2003.
19. Snoek, L. C.; Robertson, E. G.; Kroemer, R. T.; Simons, J. P. Chem Phys Lett 2000, 321, 49.
20. Hunig, I.; Kleinermanns, K. Phys Chem Chem Phys 2004, 6, 2650.
21. Chin, W.; Dognon, J. P.; Piuzzi, F.; Tardivel, B.; Dimicoli, I.; Mons, M. J Am Chem Soc 2005, 127, 707.